Study on Reservoir Characteristics and Physical Property Lower Limit of Fengcheng Formation Tight Reservoir in South Slope of Mahu Sag

Zongbin Zhang[1], Jun Qin[1], Mengyun Han[2], Zhongchen Ba[1], Xinyu Chen[1], and Jiang He[3,*]
[1]*Research Institute of Exploration and Development, Xinjiang Oilfield Company, PetroChina, Karamay, Xinjiang 834000, China*
[2]*Fengcheng Oilfield Operation District, Xinjiang Oilfield Company, PetroChina, Karamay, Xinjiang 834000, China*
[3]*State Key Laboratory of Oil and Gas Reservoir Geology and Exploitation, Southwest Petroleum University, Chengdu, 610500, China*

Keywords: Junggar Basin, Fengcheng Formation, Tight oil, Effective reservoir, Lower limit of physical properties

Abstract: Fan deltaic depositional system is developed in the Permian Fengcheng Formation of Kebai area on the south slope of Mahu sag, the reservoir with ultra-low porosity, permeability and strong heterogeneity. The characteristics and lower limit of reservoir were analyzed using core and thin section observation, pore structure test. The reservoirs are mainly developed in intergranular pores of sandy conglomerate, intergranular solution pores and unfilled half-filled pores of basalt, matrix and bainite solution pores. On the one hand, the reservoir properties are affected by sedimentation, on the other hand, it is caused by the destruction of pore space by illite, illite / Montmorillonite Mixed Minerals and other clay minerals. The lower limits of reservoir porosity of P_1f_3, $P_1f_2^1$ and $P_1f_2^2$ are 5%, 3.5% and 3.8%, respectively and the lower limits of permeability are 0.013 mD, 0.02 mD and 0.02 mD, respectively. This study discussed the controlling factors of the lower limit of reservoir properties, which provides support for the exploration of conglomerate reservoir.

1 INTRODUCTION

In recent years, unconventional resources exploration has become the focus of the industry, especially the tight sandy conglomerate oil, which has become a new highlight after shale gas. Junggar basin is a large superimposed petroliferous basin. Mahu sag in the northwest margin of Junggar basin is a well-known hydrocarbon rich sag in the world (Cao et al., 2005; Lei et al., 2017; Tao et al., 2016). The latest exploration shows that the Permian Fengcheng Formation in Kebai area of the south slope of Mahu sag has developed large-scale reservoirs of volcanic rock, sandy conglomerate, and dolomite with good exploration prospects (Zhi et al., 2019).

Reservoir lithology is complex, reservoir space type and development degree are affected by many factors, and reservoir heterogeneity is strong. At present, there is little understanding about the Permian reservoir characteristics and effective reservoirs. Effective reservoir means that the reservoir has storage and seepage capacity, and can produce liquid production with industrial value under the existing technological conditions (Gao et al., 2011; Lu, 2016). The accurate identification of effective reservoirs is meaningful for the exploration and development. At present, many methods are used to calculate the lower limit of reservoir properties, including empirical statistics method, oil bearing occurrence method, testing method, relative permeability curve combination method, physical property test method and test data constraint method (Liu et al., 2014; Xiao et al., 2004).

2 STUDY AREA

The study area is one of the most oil-gas enriched areas in Karamay Oilfield. Oil is widely distributed in Permian, Triassic, and Jurassic. Structurally, it is located on the Karamay Baikouquan fault zone, with Zaire Mountain in the West and Mahu depression in the East. There are Carboniferous, Permian Quaternary strata from bottom to top, which are very

Zhang, Z., Qin, J., Han, M., Ba, Z., Chen, X. and He, J.
Study on Reservoir Characteristics and Physical Property Lower Limit of Fengcheng Formation Tight Reservoir in South Slope of Mahu Sag.
In *Proceedings of the 7th International Conference on Water Resource and Environment (WRE 2021)*, pages 504-512
ISBN: 978-989-758-560-9; ISSN: 1755-1315

complete. Among them, Permian, Triassic and Carboniferous are in unconformity contact. The Permian can be divided into Jiamuhe (P_1j), Fengcheng (P_1f), Xiazijie (P_2X), lower Wuerhe (P_2W) and upper Wuerhe formation (P_3W). The early and middle Hercynian movement resulted in the development of unconformities of different scales among the Permian groups. The Fengcheng Formation of Permian can be divided into the first member (P_1f_1), the second member (P_1f_2) and the third member (P_1f_3) from bottom to top. The second member can be further divided into $P_1f_2^1$ and $P_1f_2^2$. Grain size of the sediments in P_1f_1 and P_1f_3 is coarse, and the lithology is mainly conglomerate and gravelly sandstone of fan delta origin. The P_1f_2 is mainly medium sandstone and fine sandstone, and a set of relatively stable overflow facies volcanic rocks are developed at the top.

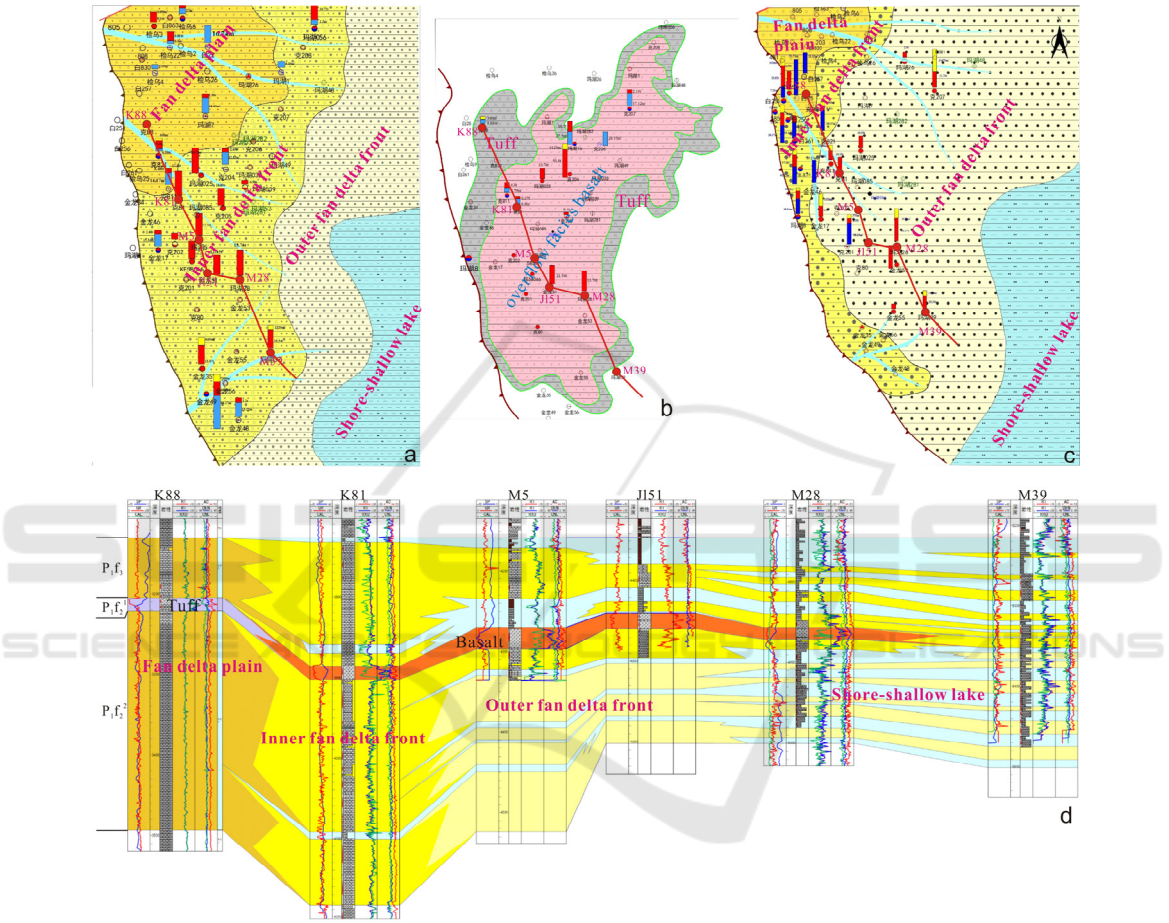

Figure 1: Sedimentary facies distribution of P_1f_3 (a), $P_1f_2^1$ (b) and $P_1f_2^2$ (b) member in Ke204 area.

3 RESERVOIR CHARACTERISTICS

3.1 Characteristics of Sedimentary Facies

The orogenic systems formed under the thrusting and napping during the development period of the foreland basin of Permian sedimentation is the material source. Through the denudation and transportation of water flow, it is dominated by terrigenous pyroclastic rocks. Through the canyon and Intermountain River, it is deposited in the fan delta near the mountain pass. Reservoir lithology is mainly sandy conglomerate, conglomerate, arenaceous small conglomerate and gravel bearing coarse sandstone of alluvial fan facies and fan delta facies (Wang et al., 2018; You, 1986).

The top of P_1f_3 formation of Permian is a set of grey and light grey lacustrine mudstone, and the lower part is fan delta front deposit with sand mud

interbedding. The deep-water environment of slope area is developed with dolomitic sandstone.

There are two kinds of sedimentary microfacies, underwater distributary channel and inter channel, in the fan delta front of P_1f_3 member. The distributary channel is composed of small conglomerate and medium coarse sandstone. The logging curve shows low GR box curve characteristics, and the SP curve shows low value characteristics, indicating high-energy sedimentary environment. The distributary channel is composed of brown or gray mudstone or silty mudstone, and the GR curve is toothed, indicating a relatively low-energy sedimentary environment. The characteristics of base level cycle show that the regional base level is low, and the accommodation space is small during the whole sedimentary period. Sand body scale of main channel is controlled by the dual factors of spin cycle and other cycle. the sand content is less in the slope area, the lateral continuity of sand body is poor, and the conglomerates at the bottom are superposed (Figure 1a).

The $P_1f_2^1$ member is a set of volcanic rock deposits. The lithology is volcanic rock extrusive deposits dominated by light gray, gray basalt or tuff. The logging curve is characterized by a large set of box curve. The main reservoir is basalt, and the reservoir is in the effusion facies. The $P_1f_2^2$ member is a set of interbedded argillaceous sandstones and mudstones. The developed dolomitic sandstones are fan delta front deposits. On the logging curve, it shows the characteristics of toothed box or bell. The reservoir lithology is mainly medium fine sandstone, and the reservoir is located in the outer front of fan delta (Figure 1b, c).

The sedimentary facies profile of K88 well to M39 well shows that the sand body structure of P_1f_3 and $P_1f_2^2$ member gradually changes from massive to interbedded from plain facies to front facies along the provenance direction, and the sand body gradually becomes thinner and thinner away from the provenance direction; overflow volcanic basalt is distributed stably in $P_1f_2^2$ member (Figure 1d).

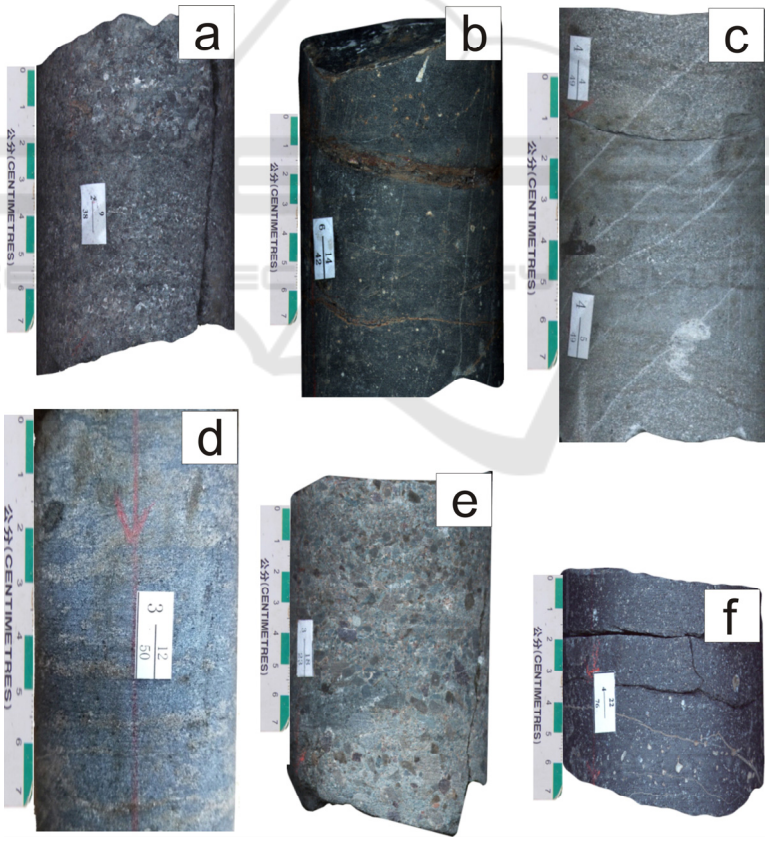

Figure 2: Lithofacies characteristics of the Fengcheng Formation. a. grey sandy conglomerate, 4393.78 ~ 4393.94m, P_1f_3 member, well JL 51; b. Dark gray basalt, 4383.00 ~ 4383.15m, $P_1f_2^1$ member, well K204; c. grey medium fine sandstone, 4929.6 ~ 4929.8m, $P_1f_2^2$ member, well M39; d. grey medium fine sandstone, 4839.50 ~ 4839.65m, $P_1f_2^2$ member, well M28; e. Grey sandy conglomerate, 3711.06 ~ 3711.20m, P_1f_3 member, well JL17; f. Grey basalt, 4423.90 ~ 4423.98m, $P_1f_2^1$ member, well M16.

3.2 Lithologic Characteristics of Reservoir

Vertically, the lithology of each member is significantly different, especially the reservoir rock type. The lithology of P_1f_3 member is sandy conglomerate, gravel bearing fine sandstone, gravel bearing argillaceous fine sandstone and fine sandstone. The size of gravels varies from 0.125 cm to 2 cm, mostly in sub angular to sub circular shape; the composition of gravel is complex, mainly tuff, accounting for 30% - 75%, followed by felsite and andesite, accounting for 3% - 12%; the main sandy component is tuff, accounting for 22% - 86%, followed by quartz, feldspar, andesite, rhyolite and basalt, accounting for 7% - 10%; the interstitial materials are mainly calcite, analcite, dolomite, etc., with the content of about 2% - 5%; the impurity bases are mainly argillaceous, micritic calcite, volcanic dust, etc., with the content of about 1% - 6%; Porous cementation is common; the rock structure is mainly composed of sand gravel structure and unequal grain sand structure, which are supported by grains; The contact between particles is mainly point-line contact; rock particles is mostly sub circular, and the sorting is poor (Figure 2 a, e).

The basalts of the $P_1f_2^1$ member are of almond like structure and glass crystal interwoven structure, in which the matrix part accounts for 30% - 97%, and the almond part accounts for 3% - 30%; the primary minerals are plagioclase, accounting for 33% - 90%, followed by pyroxene, accounting for 2% - 12%, vitrinite, accounting for 8% - 15%, and magnetite, accounting for 2% - 3%; the secondary minerals are chlorite and calcite, accounting for 12% - 54%, 3% - 25%, respectively, followed by albite, accounting for 1% - 2%, calcite, accounting for 2% - 3%, and ankerite, accounting for 2% - 5% (Figure 2b, f).

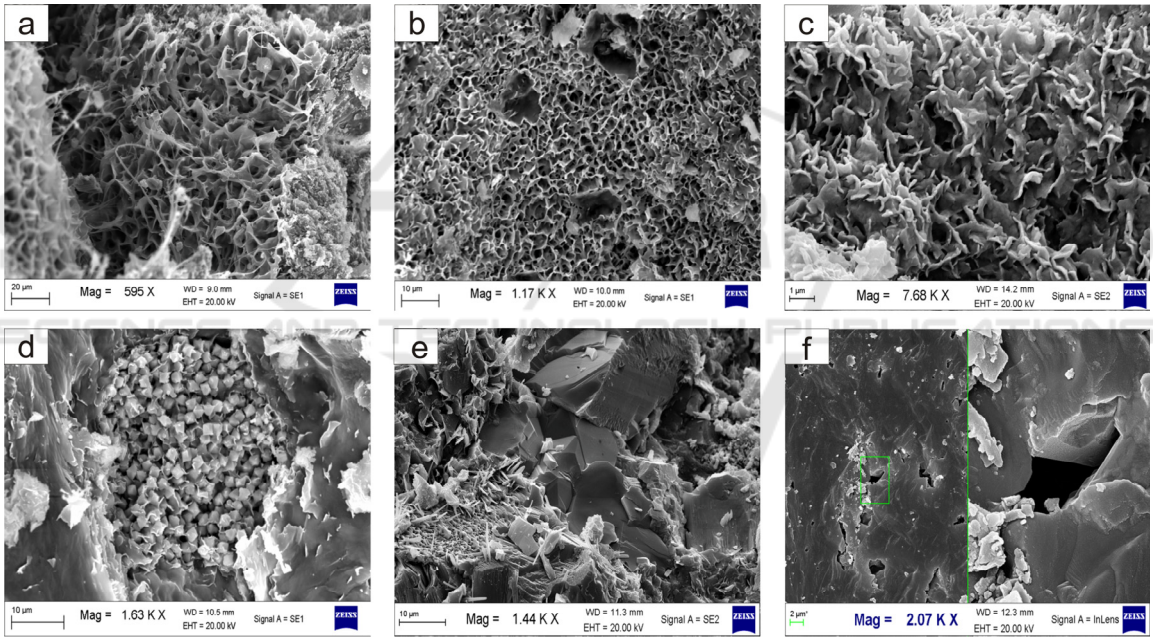

Figure 3: Typical cements habits and microstructural characteristics. a. honeycomb like illite / montmorillonite and intergranular filiform illite, 4225.42m,P_1f_2 member, well Jin35; b. honeycomb like illite / montmorillonite and intergranular filiform illite, 4225.42m, P_1f_2 member, well Jin35; c. honeycomb like illite / montmorillonite mixed layer mineral, 4844.94m,P_1f_2 member, well M28; d. pyrite intergranular pore, 4226.62m, P_1f_2 member, well Jin35; e. siliceous intergranular cement, 4933.42m, P_1f_2 member, well M28; f. dissolution pores in feldspar, 4378.82m, P_1f_3 member, well K204.

The mineral composition of the $P_1f_2^2$ member is mainly tuff, feldspar and quartz, in which tuff accounts for 54% - 73%, feldspar 10% - 15% and quartz 5% - 8%; the tuff materials in the rocks are mainly feldspar crystal chips, tuff rock chips and volcanic dust, with a small amount of glass chips; the content of intergranular argillaceous matrix is 1% ~ 4%, and the main cements are calcite and ankerite, which are distributed in a porphyritic and uneven manner, accounting for 2% ~ 5%; the cementation type is pore cementation, and the rock structure is mainly fine-grained sandy structure, supported by point-line contact particles; the particle size is

0.0625mm-0.1250mm and the roundness is sub edge to sub circle, and sorting is medium (Figure 2c, d).

Compared with sandstone, the interstitial material of conglomerate is coarser and more complex. In the framework composed of gravel particles, it is often partially or completely filled with sand particles, and in the framework composed of gravel and sand particles, it is also filled with miscellaneous base or chemical sediment (He et al., 2020). The interstitial material is divided into miscellaneous base and cement. The matrix is the material transported from the parent rock, mainly clay minerals. Cements are authigenic minerals formed by chemical precipitation during diagenesis. Cements mainly includes carbonate, zeolite, siliceous and clay minerals (Figure 3). The clay minerals are mainly illite and illite / montmorillonite. The clay filled with honeycomb or cotton wadding in the pores between the particles reduces the pore space of the reservoir, deforms the roar channel and even blocks it, which greatly reduces the permeability (Wang et al., 2017; Wang et al., 2019).

3.3 Characteristics of Reservoir Space

Pore space is an important part of reservoir rock. According to the core, thin section and physical property analysis data, the intergranular pores and dissolution pores are the main pore types in the P_1f_3 member of the wind tunnel, and a small amount of analcite dissolution pores and crushing fractures (Figure 4 a, b); The main pore types of the $P_1f_2^2$ member are unfilled semi filled pores, matrix and bainite solution pores, micro fractures, etc. (Figure 4c); The pore type of the $P_1f_2^1$ member mainly intragranular solution pore and intergranular pore, followed by micro fracture (Figure 4d, e, f). The fluorescence thin section shows that oil and gas mainly occur in the intergranular pores, intragranular dissolved pores and microfractures.

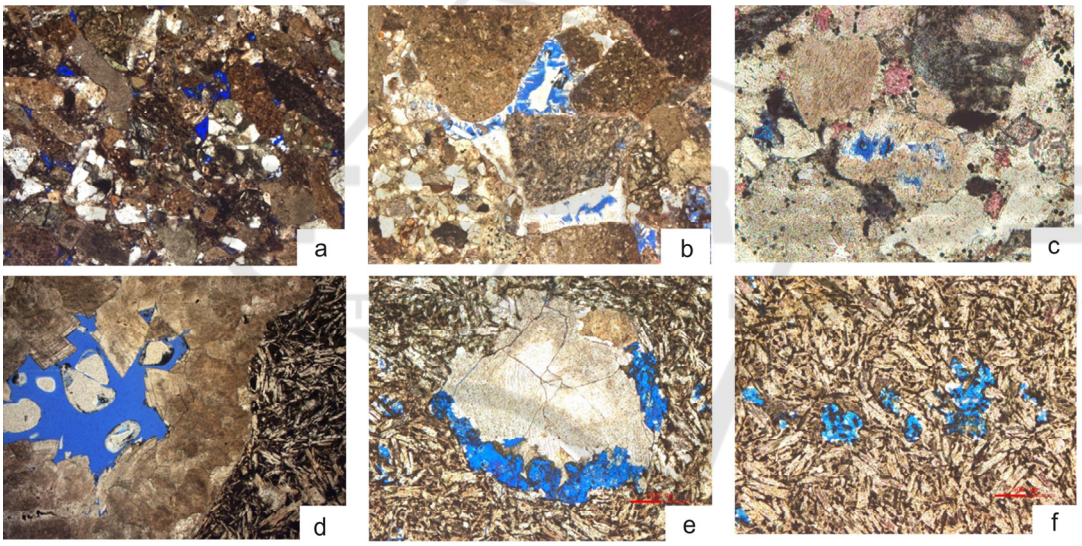

Figure 4: Microscopic pore structure of different lithofacies sample. a. the intergranular pores and dissolved pores, 4491.00m, P_1f_3 member, well Jin 35; b. residual intergranular pores and intergranular solution pores, 3709.46m, P_1f_3 member, well Jin 17; c. dolomitic fine sandstone with intragranular solution pore, 4932.07m, $P_1f_2^2$ member, well M 28; d. Semi filled pores in basalt, 4380.73m, $P_1f_2^1$ member, well K 204;e. Semi filled pores in basalt, 4445.79m, $P_1f_2^1$ member, well Jin 51; f. Matrix dissolved pores in basalt, 4449.56m, $P_1f_2^1$ member, well Jin 51.

3.4 Characteristics of Pore Structure

Among the mercury injection test of 27 rock samples in the P_1f_3 member, there are 16 samples with porosity greater than 4%, and the displacement pressure ranges from 0 MPa to 2.26 MPa. The median pressure is between 0 MPa and 18.14MPa. The maximum pore throat radius is 0-1.17 μm, most of them are less than 1.0 μm; the median radius of pore throat is 0-0.04 μm; the average of mercury removal efficiency is 16.11%. The coefficient of homogeneity is 0-0.19; the coefficient of variation ranged from 0.04 to 0.22, with an average of 0.11. The separation coefficient ranges from 0.51 to 2.53, with an average of 1.41 (Figure 5a).

The mercury injection experiment of 78 rock samples in the $P_1f_2^2$ member shows that there are 32 samples with porosity greater than 4%, and the displacement pressure ranges from 0 to 2.95 MPa, with an average of 0.57 MPa; the median pressure is between 0 and 19.48 MPa, with an average of 7.40

MPa. The maximum pore throat radius is 0-16.69 μm, and the average was 1.9 μm. Most of them are more than 1.0 μm, the median radius of pore throat is 0-0.12μm, the average was 0.05 μm, the mercury removal efficiency was 10.32% - 38.03%, with an average of 24.92%. The homogenization coefficient is between 0 and 0.19, with an average of 0.12. The coefficient of variation ranged from 0.04 to 0.29, with an average of 0.15. The separation coefficient ranges from 0.51 to 3.18, with an average of 1.81 (Figure 5b).

The results of mercury injection experiments on three rock samples in the $P_1f_2^1$ member show that, two samples with porosity greater than 4% were selected, and the displacement pressure was between 2.67 MPa and 2.95 MPa, with an average of 2.81 MPa. The median pressure is 6.22-11.41 MPa, with an average of 9.58 MPa. The maximum pore throat radius is 0.25 μm -0.28 μm. Most of them are less than 1.0 μm. The median radius of pore throat ranged from 0.06 μm to 0.12 μm, 0.83 on average μm. The mercury removal efficiency ranged from 19.76% to 21.77%, with an average of 20.76%. The homogeneity coefficient is 0.16. The coefficient of variation was 0.07. The separation coefficient ranges from 0.89 to 0.94, with an average of 0.91 (Figure 5c).

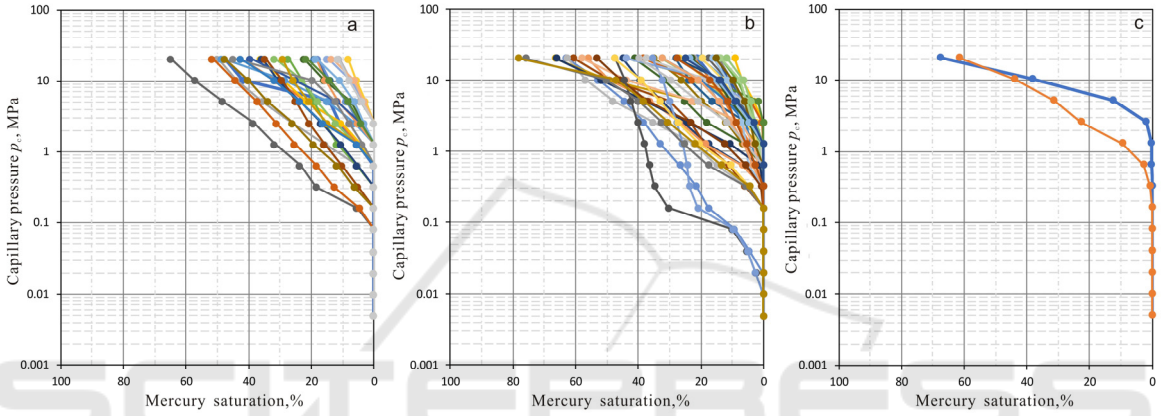

Figure 5: Typical mercury-injection curves for each member. a. P_1f_3 member; b. $P_1f_2^2$ member; c. $P_1f_2^1$ member.

4 RESERVOIR PHYSICAL PROPERTY AND LOWER LIMIT OF EFFECTIVE RESERVOIR

4.1 Physical Properties of Reservoir

The physical property test of the core samples of the P_1f_3 member shows that the minimum porosity of the core matrix is 1.7%, and the maximum porosity is 12.41%; The main distribution range of porosity is 4% ~ 7%, with an average of 5.23%; The porosity of reservoir is 5.3% ~ 12.41%, with an average of 7.13%; the minimum matrix permeability is 0.01 mD; the main distribution range is 0.02 mD ~ 0.07 mD, and the average is 0.06 mD; the reservoir analysis permeability is 0.12 mD ~ 43.61 mD, and the average is 0.74 mD.

The minimum matrix porosity of the $P_1f_2^1$ member is 1.7%, and the maximum porosity is 10.81%; the main distribution range of porosity is 2 ~ 5%, with an average of 4.56%; the porosity of reservoir analysis is 3.8% ~ 10.81%, with an average of 6.64%; the minimum matrix permeability is 0.01 mD, the main distribution range is 0.02 ~ 0.07 mD, the average is 0.09 mD; the reservoir analysis permeability is 0.13 mD~ 34.21 mD, the average is 2.73 mD.

The minimum matrix porosity of $P_1f_2^2$ member is 1.9%, and the maximum is 8.81%; the main distribution range of porosity is 2 ~ 5%, with an average of 4.18%; the porosity of reservoir is ranges 3.0% ~ 8.81%; the minimum matrix permeability is 0.02 mD, the maximum is 0.47 mD, the main distribution range is 0.02 ~ 0.07 mD, the average is 0.04 mD; the reservoir analysis permeability is 0.03 mD ~ 0.47 mD, the average is 0.07 mD.

4.2 Determination of Lower Limit of Physical Properties of Effective Reservoir

It is a complex work to determine the lower limit of reservoir parameters, which is related to the geological conditions. Different methods may lead to different conclusions (Liu et al., 2014; Xiao et al.,

2004). The reservoir characteristics of Fengcheng Formation are obvious, and the reservoir characteristics of different structures and different layers are different. Study on the lower limit of reservoir physical properties, then evaluate the reservoir effectiveness.

4.2.1 Lower Limit of Porosity

The relationship between porosity and permeability in different section is different.

In the P_1f_3, porosity is positively correlated with permeability in the middle and high porosity section, which has the characteristics of porous reservoir. The intersection points of porosity and permeability in low porosity section are scattered. According to the change of intersection curve when porosity is 5%, it is considered that 5% is the lower limit of porosity, and the corresponding permeability is 0.013 mD (Figure 6 a, d).

In the $P_1f_2^1$, porosity and permeability are exponential in medium and high porosity section, and have the characteristics of pore type reservoir, and the relationship between porosity and permeability is poor power relationship in low porosity section. According to the transition of intersection curve when porosity is 3.5%, it is considered that 3.5% is the lower porosity limit in the $P_1f_2^1$, and the corresponding permeability lower limit is 0.02 mD (Figure 6 b, e).

In the $P_1f_2^2$, the linear correlation between porosity and permeability shows the characteristics of porous reservoir. The intersection points of porosity and permeability data in low porosity section are scattered, and the relationship between porosity and permeability is poor. According to the change of intersection curve when the porosity is 3.8%, and the corresponding lower limit of permeability is 0.02 mD (Figure 6 c, f).

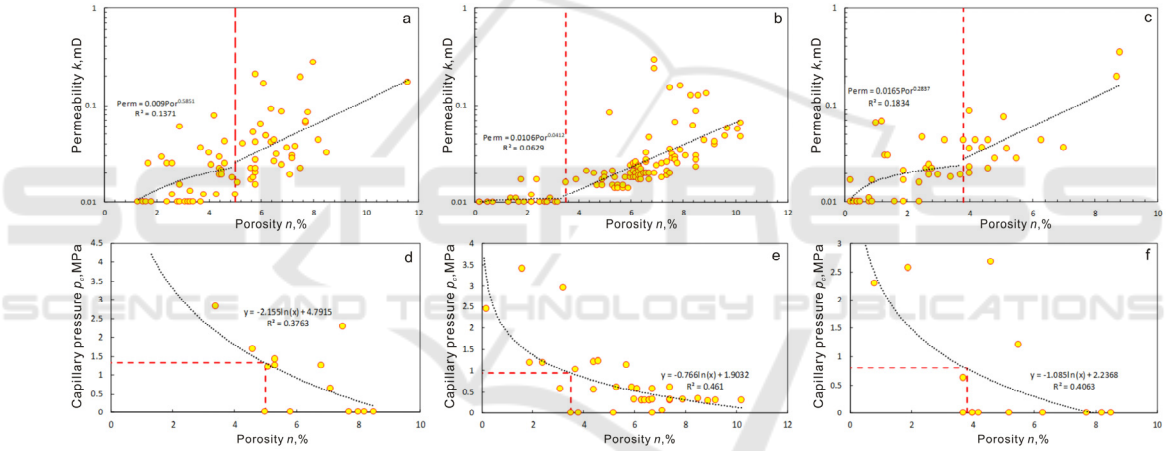

Figure 6: Correlation diagram of core porosity with permeability and mercury injection displacement pressure. a, d. P_1f_3 member; b, e. $P_1f_2^1$ member; c, f. $P_1f_2^2$ member.

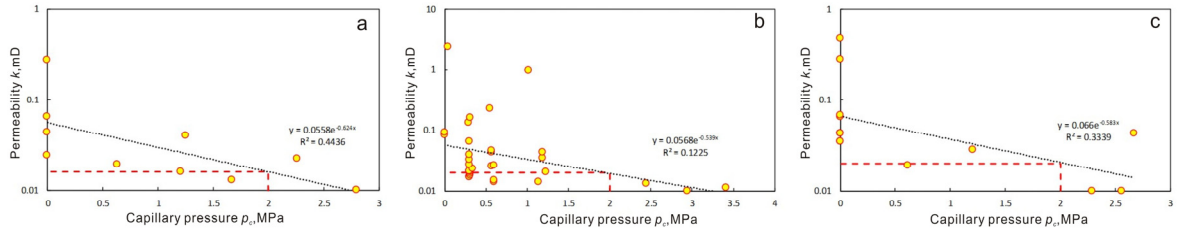

Figure 7. Correlation diagram of permeability with mercury injection displacement pressure. a. P_1f_3 member; b. $P_1f_2^1$ member; c. $P_1f_2^2$ member.

4.2.2 Lower Limit of Porosity

The throat size controls the seepage ability, the critical pore throat radius for the largest oil molecule in tight oil reservoir is 54 nm. According to the relationship between displacement pressure and permeability in the experimental parameters of core mercury injection. There is a good power relationship between the permeability and displacement pressure of the P_1f_3 member, and the correlation coefficient is high. With the increase of displacement pressure, the permeability decreases sharply. When the displacement pressure of the P_1f_3 member increases to 2 MPa, the core permeability changes slowly, indicating that the flow resistance of fluid in the micro pore throat increases, The fluid flow state tends to be static. Therefore, the permeability at this time is used as the lower limit to judge whether the reservoir still has the ability of fluid seepage, and the lower limit of permeability of the P_1f_3 member is 0.013 mD (Figure 7a).

There is a good power relationship between permeability and displacement pressure. After the displacement pressure increases to 2 MPa, the core permeability changes slowly, which indicates that the flow resistance of fluid in the micro pore throat increases, and the flow state of fluid tends to be static. Therefore, the permeability at this time is used as the lower limit to judge whether the reservoir still has the ability of fluid seepage, and the lower limit of permeability of the $P_1f_2^1$ member is 0.02 mD (Figure 7b).

There is a good power relationship between permeability and displacement pressure. When the displacement pressure increases to 2 MPa, the core permeability changes slowly. Therefore, the permeability at this time is used as the lower limit to judge whether the reservoir still has the ability of fluid seepage, and the lower limit of permeability of the $P_1f_2^2$ member is 0.02 mD (Figure 7c).

5 CONCLUSION

1. The Permian fan delta deposits are developed. The lithology of the fan delta front of P_1f_3 and $P_1f_2^2$ members is mainly sandy conglomerate, gravel bearing fine sandstone, gravel bearing argillaceous fine sandstone and fine sandstone. In $P_1f_2^1$ member, volcanic exhalative deposits and basalt are developed.

2. The pore types in sandy conglomerate are mainly intergranular pores and dissolution pores, with a small amount of analcite dissolution pores and crushing fractures. The pore types in volcanic rocks are mainly unfilled semi filled pores, matrix and bainite dissolution pores, micro fractures, etc.

3. The structural characteristics of the original deposition of sandy conglomerate leads to poor preservation conditions of original pores. The development of authigenic cements, especially illite, illite / montmorillonite mixed minerals and other clay minerals in the later stage, lead to the destruction of pore space in the main reservoir section, the deformation of roar channel, even plugging, and greatly reduced permeability.

4. The lower limits of reservoir porosity of P_1f_3, $P_1f_2^1$ and $P_1f_2^2$ member are 5%, 3.5% and 3.8%, respectively. The lower limits of permeability are 0.013 mD, 0.02 mD and 0.02 mD, respectively.

ACKNOWLEDGMENT

This study was financially supported by the Science and Technology Cooperation Project of the CNPC-SWPU Innovation Alliance, Science and Technology Agency of Sichuan province (No.18YYJC1120), China Postdoctoral Science Foundation (No. 2017M623059) and the Open Fund of State Key Laboratory of Oil and Gas Reservoir Geology and Exploitation, Southwest Petroleum University (CN). We would like to thank the Southwest Oil & Gas Field Branch Company Ltd. PetroChina for providing shale samples and data.

REFERENCES

Cao, J., Zhang, Y., Hu, W., Yao, S., Wang, X., & Zhang, Y. (2005). The Permian hybrid petroleum system in the northwest margin of the Junggar basin, northwest China. *Marine & Petroleum Geology, 22*(3), 331-349.

Gao, Y., Jiang, Y. Q., & Yang, C. C. (2011). Minimum flow pore throat radius for determination of the lower limits of parameters in low permeability reservoir. *Science & Technology Review, 29*(4), 34-38.

He, J., Tang, H., Wang, L., Yang, Z., & Wan, B. (2020). Genesis of heterogeneity in conglomerate reservoirs: insights from the Baikouquan formation of Mahu sag, in the Junggar basin, China. *Petroleum Science and Technology, 39*(2), 1-19.

Lei, D., Chen, G., Liu, H., Li, X., Abulimit, Ta, K., & Cao, J. (2017). Study on the forming conditions and exploration fields of the Mahu giant oil (gas) province, Junggar basin. *Acta Geologica Sinica.91*(7), 1604-1619.

Liu, M. L., Feng, Z. P., & Cai, Y. L. (2014). Present situation and developmental trend of the research on methodology for determination of physical properties cut-off of an effective reservoir. *Acta Geologica Sichuan, 34*(1) :9-13.

Lu, Y. Z. (2016). New method for evaluating the effective thickness of carbonate reservoir on well logging data. *Progress in Geophysics, 31*(5), 1959-1964.

Tao, K., Cao, J., Wang, Y., Ma, W., Xiang, B., & Ren, J. (2016). Geochemistry and origin of natural gas in the petroliferous Mahu sag, Northwestern Junggar basin, NW China: carboniferous marine and Permian lacustrine gas systems. *Organic Geochemistry,100*, 62-79.

Wang, M., Zhang, Z., & Zhou, C. (2018). Lithological characteristics and origin of alkaline lacustrine of the Lower Permain Fengcheng Formation in Mahu Sag, Junggar Basin. *Journal of Palaeogeography, 20*(1), 147-162.

Wang, M., Tang, H., Feng, Z., Shu, L., & Hao, L. (2017). Controlling factor analysis and prediction of the quality of tight sandstone reservoirs: a case study of the He8 member in the eastern sulige gas field, ordos basin, China. *Journal of Natural Gas Science & Engineering, 46*, 680-698.

Wang, M., Tang, H., Tang, H., Liu, S., & Cheng, Y. (2019). Impact of differential densification on the pore structure of tight gas sandstone: evidence from the Permian Shihezi and Shanxi formations, eastern Sulige gas field, ordos basin, China. *Geofluids, 2019*(2), 1-25.

Xiao, S. H., Zhou, W., & Wang, Y. C. (2004). Method for determining the lower limits of effective reservoirs. *Journal of Chengdu University of Technology, 31*(6), 672-674.

You, X. (1986). Discuss on the lower Permian Fengcheng Formation in the northwest margin of Junggar Basin. *Xinjiang Petroleum Geology, 7*(1), 47-52.

Zhi, D., Song, Y., & He, W. (2019). Geological characteristics, resource potential and exploration direction of shale oil in Middle-Lower Permian, Junggar Basin. *Xinjiang Petroleum Geology, 40*(4), 389-401.